J Mater Sci (2018) 53:1978–1986

Electronic materials

The visible light hydrogen production of the Z-Scheme Ag_3PO_4/Ag/g-C_3N_4 nanosheets composites

Mingzhu You[1], Jiaqi Pan[1], Chunyan Chi[1], Beibei Wang[1], Weijie Zhao[1,2], Changsheng Song[1], Yingying Zheng[1], and Chaorong Li[1,*]

[1] Department of Physics and Key Laboratory of ATMMT Ministry of Education, Zhejiang Sci-Tech University, Hangzhou 310018, People's Republic of China

[2] School of Medical and Pharmaceutical Engineering, Taizhou Vocational & Technical College, Taizhou, People's Republic of China

Received: 18 July 2017
Accepted: 18 September 2017
Published online: 22 September 2017

ABSTRACT

The Z-Scheme Ag_3PO_4/Ag/g-C_3N_4 nanosheets composites are synthesised via simple annealing and anion-exchange precipitation method. The obtained samples are characterized by SEM, XRD, TEM, XPS, UV–Vis and PL, which imply that the Z-Scheme Ag_3PO_4/Ag/g-C_3N_4 structure has been prepared successfully. The photocatalytic activity of the as-prepared Ag_3PO_4/Ag/g-C_3N_4 nanosheets composites displays a remarkable enhancement after the Ag_3PO_4/Ag nanoparticles being introduced by the hydrogen production under visible light. Further, the Z-Scheme structure of the sample and the lamellar structure of the C_3N_4 are considered as the main reasons for the enhancement.

Introduction

As an apinoid and almost infinite source, solar energy has been explored by heaps of ways, such as solar cells, solar water heater or simulate chlorophyll [1, 2], especially the solar hydrogen production, with the high combustion heat, non-pollution and directly utilized properties of the H_2, is considered as an ideal way to take advantage of the solar energy. Since it was first reported in 1972, lots of significant results have been achieved [3–5]. In view of the high proportion of the visible light in sunlight, in recent years, most researchers have focused on visible light hydrogen production photocatalyst, such as $InVO_4$ [6], $LaTiO_2N$ [7] and CdS, and have obtained series of achievements [8]. In those photocatalytic materials, the graphitic carbon nitride (g-C_3N_4), with low cost and physical–chemical stability, has been demonstrated to be an especially promising photocatalyst for the splitting of water into H_2 and decomposing organic pollutants using solar energy [9–11]. Compared with most traditional materials, the g-C_3N_4 with unique electronic band structure could be synthesized though simple and environment friendly methods and has achieved prominent results [12–14]. As known, how to decrease the recombination rate of photo-generated electron–hole pairs of g-C_3N_4 is one of the most efficient ways to improve the photocatalysis. In view of this, lots of researchers have tried a variety of attempts. As reported in early literatures, loading with noble metals (Au, Pt) is a valid way, up

Address correspondence to E-mail: crli@zstu.edu.cn

DOI 10.1007/s10853-017-1612-6

to now, many synthetic methods for the fabrication of noble metal/g-C_3N_4 photocatalysts have been developed [15, 16]. However, the preparation cost would be dearly for most minor enterprises, and restrict those photocatalysts being used in practical application. On the other hand, the heterojunction modification is considered as another ideal way, and lots of researches have been reported, such as Hao et al. [17] have prepared macro/mesoporous g-C_3N_4/TiO_2 heterojunction for enhancing the visible light photocatalysts, Karimi-Nazarabad et al. [18] have prepared the semiconductor coupling g-C_3N_4/WO_3 for solar light-driven photocatalysis, or others ways as g-C_3N_4/$SrTiO_3$ [19], g-C_3N_4/Bi_2WO_6 [20] and g-C_3N_4/In_2O_3 [21]. For above studies, the heterojunction structure could promote the photon-generated carriers that separate and increase the photocatalytic process efficiently, and indicate that the suitable composite modification is an efficient way in future researches.

In numerous materials, the Ag_3PO_4, with easy preparation and unique band gap structure [22, 23], is expected as a promising visible-light-active photocatalyst. Compared with Au or Pt, the preparation and cost of the Ag_3PO_4 is easy and cheap [24]. After being introduced into the C_3N_4 system, those could form a heterojunction and promote the photon-generated electron–hole pairs separating efficiently [25–27]. What is more, the surface of Ag_3PO_4 could decompose to form a sparse Ag shell, which could make the composites to generate a Z-Scheme structure to quench the photon-generated electron (from the conductive band of Ag_3PO_4) and hole (from the valence band of the C_3N_4) quickly, that is much more efficient than the traditional heterojunction, Lu et al. have prepared the Z-Scheme WO_3/Ag_3PO_4 composites with enhanced visible light photocatalytic performances [28], Fan et al. have obtained the Z-Scheme visible-light-driven Ag_3PO_4/MoS_2 nanocomposites [29], Dai groups have synthesized the Z-Scheme Bi_2MoO_6/Ag_3PO_4 composites for enhanced photocatalysis [30], and so on [31, 32]. In addition, the sparse Ag shell on the surface of the Ag_3PO_4 could prevent the degradation of the Ag_3PO_4 and improve the photocatalytic stability, which is another advantage for the Ag_3PO_4 modification [33, 34].

Herein, we prepared the Z-Scheme Ag_3PO_4/Ag/g-C_3N_4 nanosheets photocatalysts by simple annealing and anion-exchange precipitation methods. The as-prepared Z-Scheme Ag_3PO_4/Ag/g-C_3N_4 nanosheets composites exhibit an obvious enhancement of hydrogen production under visible light irradiation. Further, the visible light hydrogen production mechanism of the Z-Scheme Ag_3PO_4/Ag/g-C_3N_4 composites is discussed.

Experimental

Materials

All the chemicals were analytical grade and used without further purification. Silver nitrate ($AgNO_3$), sodium phosphate dibasic dodecahydrate ($Na_2HPO_4{\cdot}12H_2O$) and melamine ($C_3H_6N_6$) were purchased from Sigma-Aldrich. The deionized water was produced from a Millipore Milli-Q water purification system and used throughout the whole experiments.

Synthesis

The bulk g-C_3N_4 was synthesized by thermal polycondensation of melamine. Typically, 10 g of melamine powder was put into an alumina crucible with a cover and heated to 550 °C at a rate of 5 °C/min and maintained for 4 h. The resultant yellow product was collected and milled into powder. Then, the as-prepared bulk g-C_3N_4 (1 g) was mixed with 10 mL of H_2SO_4 (98 wt%) in a 50-mL flask and stirred for 8 h at room temperature. Then, the mixture was poured into 100 mL of deionized water slowly and sonicated for exfoliation. In this process, the temperature increased rapidly and the color changed from yellow to light yellow. The obtained suspension was then subjected to 10 min of centrifugation at 3000 rpm to remove any un-exfoliated g-C_3N_4. The obtained light yellow suspension was centrifuged, washed thoroughly with deionized water to remove the residual acid, and finally dried at 80 °C in air for 12 h.

The Z-Scheme Ag_3PO_4/g-C_3N_4 nanosheets composites were prepared by a facile chemisorption method. In brief, 10 mg g-C_3N_4 nanosheets was dispersed into deionized water (20 mL) with sonication for 1 h, and then 0.03 M $AgNO_3$ (0, 5, 10, 15 ml) was added into the g-C_3N_4 dispersion to obtain a homogeneous phase after stirring for 60 min at room temperature. The electrostatically driven assembly of positively charged Ag^+ ions on the negatively charged g-C_3N_4 sheets was achieved. And then 0.05 M $Na_2HPO_4{\cdot}12H_2O$ (0, 7.5, 15, 22.5 ml) was

added dropwise into the $Ag^+/g\text{-}C_3N_4$ dispersion, under magnetic stirring for 60 min, then generating a yellow–brown precipitate. All the processes proceed on the illumination, so parts of Ag_3PO_4 decomposed to the Ag and deposited on the surface to generate a sparse Ag shell. The obtained Z-Scheme Ag_3PO_4/Ag/g-C_3N_4 composites were washed with distilled water and absolute ethanol for three times, and finally dried at 60 °C for 8 h. Then, the samples with different concentration of Ag_3PO_4/Ag were denoted as Ag-CN-0(0 ml $AgNO_3$ + 0 ml $Na_2HPO_4{\cdot}12H_2O$), Ag-CN-1(5 ml $AgNO_3$ + 7.5 ml $Na_2HPO_4{\cdot}12H_2O$), Ag-CN-2(10 ml $AgNO_3$ + 15 ml $Na_2HPO_4{\cdot}12H_2O$) and Ag-CN-3(15 ml $AgNO_3$ + 22.5 ml $Na_2HPO_4{\cdot}12H_2O$).

Characterizations

The phase structures of the samples were characterized by X-ray diffraction (XRD) on a Bruker D8 diffractometer (1.5406 Å, 40 kV and 40 mA). The morphology of the samples was characterized by the field-emission scanning electron microscope (FESEM, Hitachi S-4800). The crystal structures were characterized by the transmission electron microscopic (TEM) images (JEM-2100 microscope, 200 kV). X-ray photoelectron spectra (XPS) were measured by a Kratos Axis Ultra system (ESCALAB250).

Photocatalytic performance measurements

The photocatalytic hydrogen evolution was performed in Labsolar III system (Beijing Perfectlight Technology Co. Ltd.). An outer irradiation-type photoreactor (Pyrex reaction vessel) was connected to a closed gas circulation and an evacuation system. The evolved gases were analyzed by an online gas chromatograph (GC) equipped with a thermal conductivity detector (TCD) and molecular sieve (5 Å pore size). High purity Ar was used as the carrier gas. In the experiment, 50 mg of photocatalyst was dispersed into 100 mL deionized water containing sacrificial reagent (20 ml triethanolamine, TEOA). Before reaction, the whole system was pumped out to remove the dissolved air. A 300-W Xe lamp, equipped with a UV cutoff filter, was used as the visible light source (> 420 nm). A circulation of water with an external cooling coil was conducted to maintain the temperature of suspension at about 25 °C.

Results and discussion

Figure 1 is the morphology of the as-prepared g-C_3N_4 nanosheets and Ag_3PO_4/Ag/g-C_3N_4 nanosheets composites. Figure 1a is the SEM of the pure C_3N_4 (Ag-CN-0). As seen, the as-prepared C_3N_4 is lamellate, which could provide large surface area for the growth of the Ag_3PO_4/Ag nanoparticles and the reaction interfaces for photocatalysis. As shown in Fig. 1b–d, it is obvious that the Ag_3PO_4/Ag nanoparticles, with the diameter about 300 nm, are introduced and deposit on the surfaces of the C_3N_4 nanosheets successfully, and which increase with the solution concentration.

Further, the crystal structures of the Ag_3PO_4/Ag/g-C_3N_4 nanosheets composites are characterized by TEM and shown in Fig. 2. As revealed, the C_3N_4 nanosheets are thin, and the Ag_3PO_4/Ag nanoparticles with diameter of about 300 nm deposit on it, which is corresponded to the SEM. Figure 2b and c is the HRTEM of the Ag_3PO_4 and g-C_3N_4. As shown, the lattice spacing of 0.241 and 0.328 nm is ascribed to the (211) plane of the Ag_3PO_4 and (002) plane of the C_3N_4 [35]. Restricted by the crystallinity and thickness of the Ag shell, the HRTEM of the Ag shell could not be provided, which would be proved in XRD and XPS.

The phase structure of the as-prepared Ag_3PO_4/Ag/g-C_3N_4 composites with different concentration of Ag_3PO_4/Ag is characterized by XRD and shown in Fig. 3. As displayed, all of the samples exhibit a distinct diffraction peak at 27.7°, which can be indexed to the (002) plane of the g-C_3N_4 (JCPDS-87-1526). With the Ag_3PO_4/Ag nanoparticles being introduced, the samples exhibit obvious diffraction peaks at $2\theta = 20.8°$, 29.7°, 33.3°, 36.6°, 42.5°, 47.8°, 52.7°, 55.1°, 57.3°, 61.7°, 69.9°, 71.9°, and 73.8°, which could be indexed to the (110), (200), (210), (211), (300), (310), (222), (320), (321), (400), (420), (421) and (332) planes of the Ag_3PO_4 phase (JCPDS-02-0931), and increase with the concentration of the reaction solution. What is more, the diffraction peak of Ag at 38.1° could be observed and indexed to (111) plane of the Ag (PDF-04-0783) [35]. Limited by the crystallinity, the diffraction peak of Ag is weak, while increases with the reaction solution, that is similar to the Ag_3PO_4. Those above indicate that the Ag may adhere to the Ag_3PO_4.

Furthermore, the components and surface properties of the Ag_3PO_4/Ag/g-C_3N_4 nanosheets

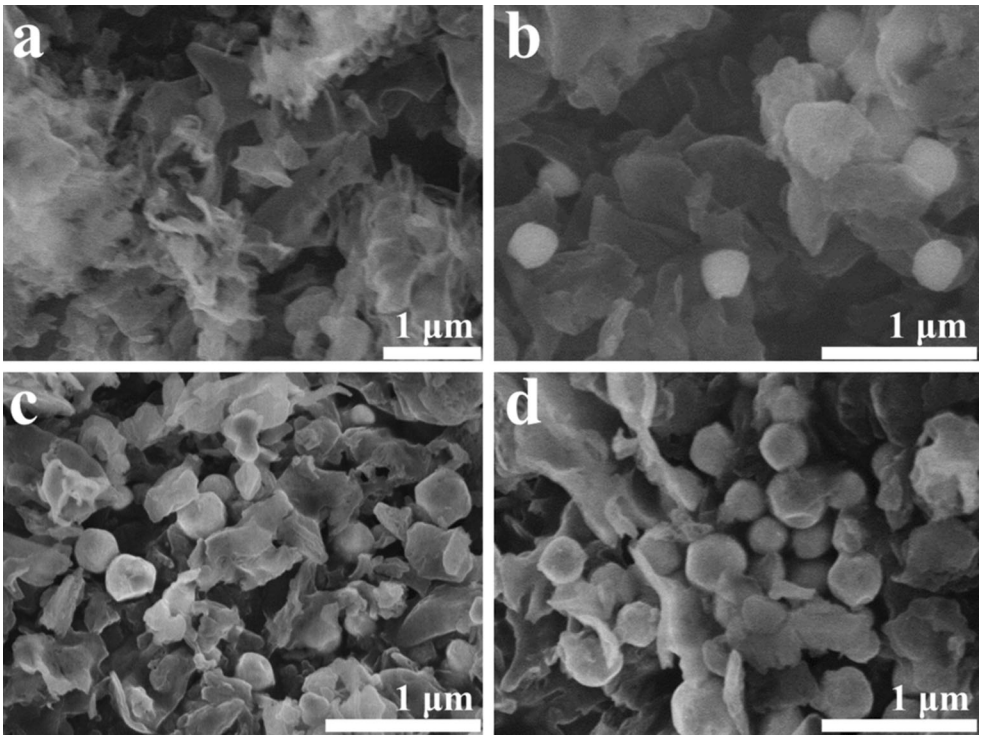

Figure 1 The SEM of as-prepared g-C_3N_4 nanosheets and Ag_3PO_4/Ag/g-C_3N_4 nanosheets composites with different ratio.

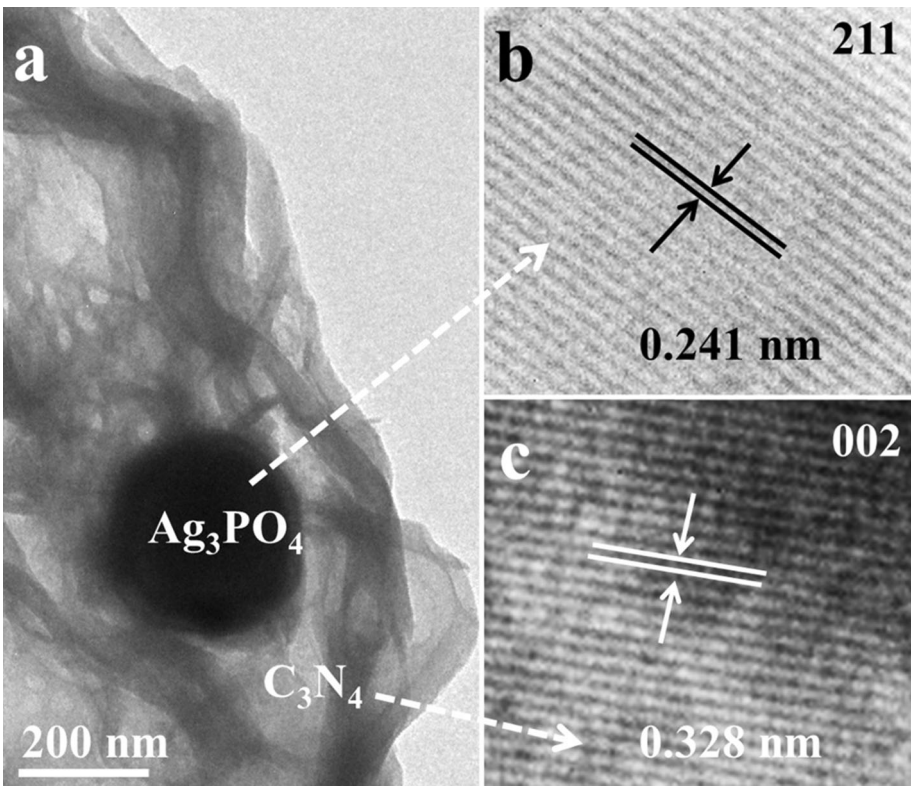

Figure 2 The TEM of Ag_3PO_4/Ag/g-C_3N_4 nanosheets composites, **a** the TEM of the sample, **b** the HRTEM of the Ag_3PO_4 and **c** the HRTEM of the C_3N_4.

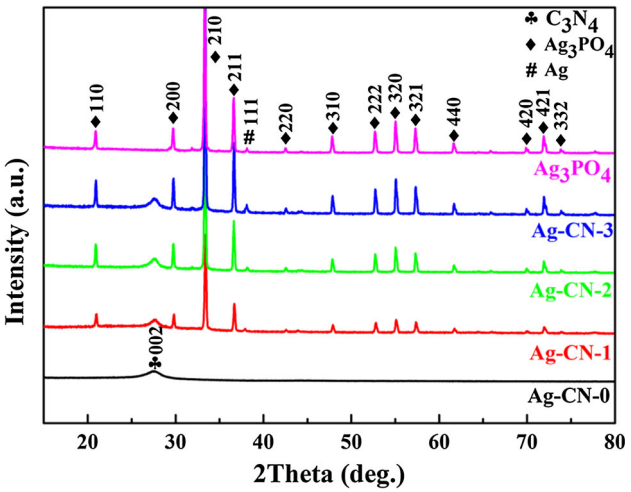

Figure 3 The XRD of the samples with different concentration of Ag_3PO_4/Ag.

composites (Ag-CN-2) are characterized by XPS. Figure 4 is the XPS spectra of the as-prepared $Ag_3PO_4/Ag/g\text{-}C_3N_4$ nanosheets composites. Figure 4a is the full survey spectrum, which indicates the presence of phosphorus (P 2p), carbon (C 1s), silver (Ag 3d, 3 g), nitrogen (N 1s) and oxygen (O 1s) in the $Ag_3PO_4/Ag/g\text{-}C_3N_4$ nanosheets composites. Figure 4b is the high-resolution Ag 3d spectrum. As revealed, two distinct peaks at 368.3 eV (Ag $3d_{5/2}$) and 374.4 eV (Ag $3d_{3/2}$) could be ascribed to the Ag in the composites. Further, the Ag $3d_{5/2}$ peak could be divided into two peaks at 368.1 and 368.8 eV, while the Ag $3d_{3/2}$ peak could be divided into two peaks at 374.1 and 374.8 eV, respectively. As shown, the peaks of 368.1 and 374.1 eV could be assigned to Ag^+, while the peaks of 368.8 and 374.8 eV could be attributed to metallic Ag(Ag^0), which is corresponding to previous literatures [36]. Figure 5c is the high-resolution C 1s spectrum. As revealed, the curve could be fitted into two peaks, the peaks located at 284.8 eV could be ascribed corresponding to the C–C bond with sp^2 orbital, and the peak located at 288.4 eV could be assigned to the carbon atoms in

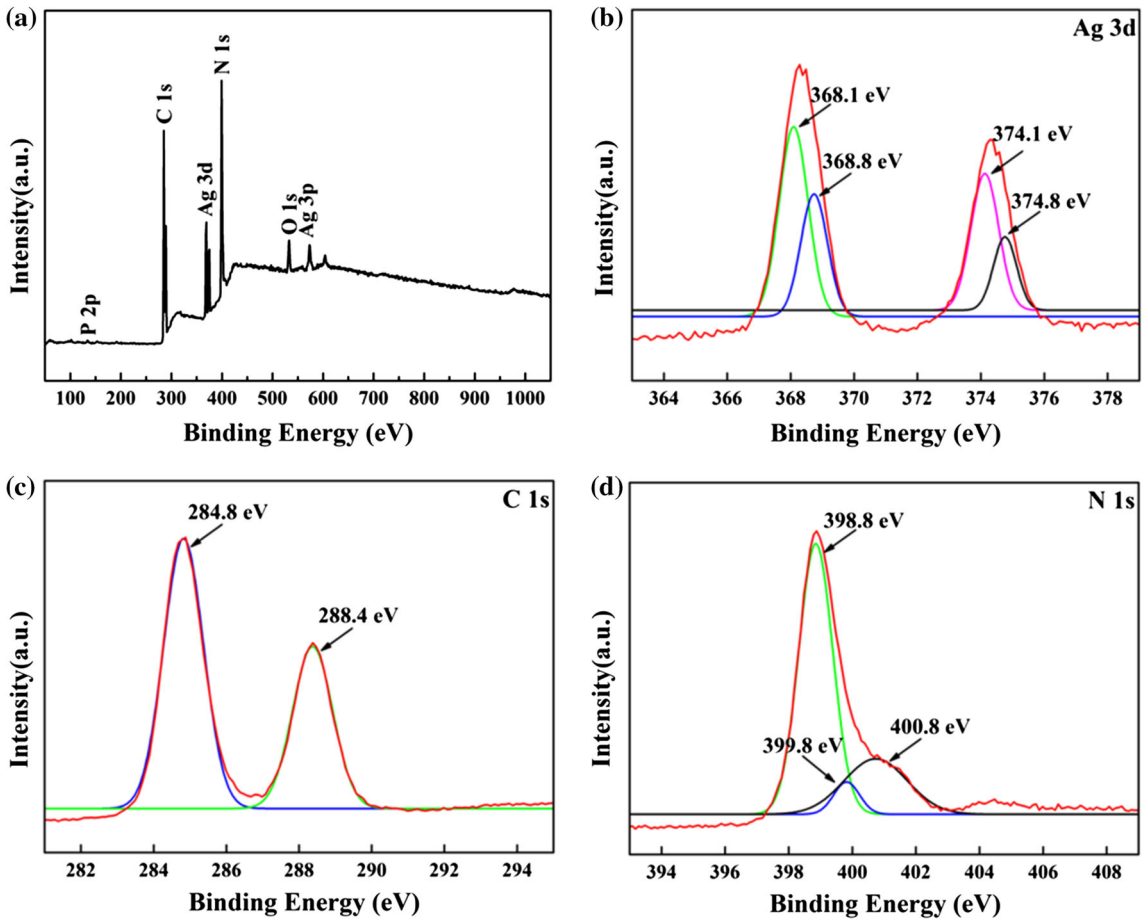

Figure 4 The XPS spectra of the $Ag_3PO_4/Ag/g\text{-}C_3N_4$ nanosheets composites, **a** full survey, **b** Ag 3d spectrum, **c** C 1s spectrum and **d** N 1s spectrum.

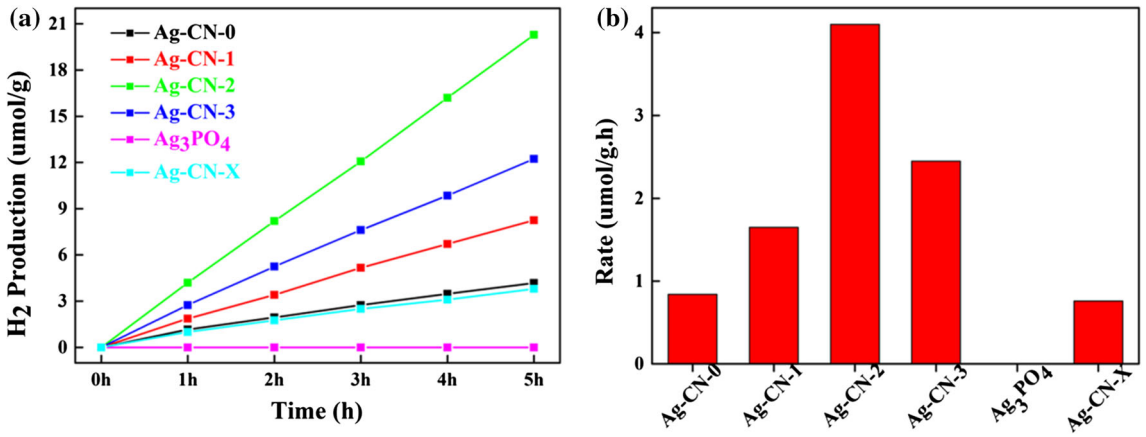

Figure 5 Visible light hydrogen production activity **a** different ratio of Ag PO_4/Ag/g-C_3N_4 composites, **b** the histogram of the samples.

N-containing aromatic rings [37]. Moreover, as shown in Fig. 4d, the N 1s spectrum could be divided into three different nitrogen species, namely the peaks located at 398.8, 399.8 and 400.8 eV could be assigned to the C=N–C, N–$(C)_3$ and C–N–H, respectively [37]. Compared with the unmodified pure g-C_3N_4 (shown in ESI Fig. S1), the 0.2 eV of the peak shift (N 1s) indicates that the modification has formed [38]. The results of XPS indicate the existence of the Ag_3PO_4, metal Ag and g-C_3N_4 units, which are the elementary building blocks of Ag_3PO_4/Ag/g-C_3N_4 and correspond to the XRD.

All the above results manifest that the Ag_3PO_4/Ag nanoparticles have deposited on the surfaces of g-C_3N_4 nanosheets.

The photocatalytic performances for hydrogen production of the different Ag_3PO_4/Ag/g-C_3N_4 nanosheets composites are displayed in Fig. 5. All experiments are carried out under visible light irradiation (> 420 nm), and the TEOA aqueous solution is employed as the sacrificial agent. As revealed, the pure g-C_3N_4 nanosheets exhibit a weaker hydrogen production of (~ 0.84 μmol/g·h), which could be ascribed to the intrinsic hydrogen production property of the g-C_3N_4. It is obvious that the hydrogen production increases with the ratio of Ag_3PO_4/Ag, and get an optimal value at the Ag-CN-2 (~ 4.1 μmol/g·h), then decreases. By calculating, the hydrogen production of the Ag_3PO_4/Ag/g-C_3N_4 is about five times of the pure g-C_3N_4. As a control group, the Ag_3PO_4/Ag nanoparticles and g-C_3N_4 nanosheets are simply mixed in solution and labeled as Ag-CN-X (the ratio is the same as the Ag-CN-2). However, the hydrogen production of the Ag-CN-X is similar as the pure g-C_3N_4, and which is helpful to explain the mechanism of the Z-Scheme structure. It is obvious that the suitable concentration of the Ag_3PO_4/Ag and the unique structure of the Ag_3PO_4/Ag/g-C_3N_4 could increase the hydrogen production efficiently.

Figure 6 shows the UV–visible absorption spectra of Ag_3PO_4/Ag/g-C_3N_4 composites with different amount of Ag_3PO_4/Ag. As shown, the absorption band of pure g-C_3N_4 locates at approximately 460 nm, which is ascribed to the intrinsic band gap of the g-C_3N_4. Then, the absorption of the composites displays an obviously red-shift and increasing with the increasing concentration of the Ag_3PO_4/Ag in visible light area, which could be attributed to the band gap of the Ag_3PO_4 (2.4 eV) [39]. These red-shift

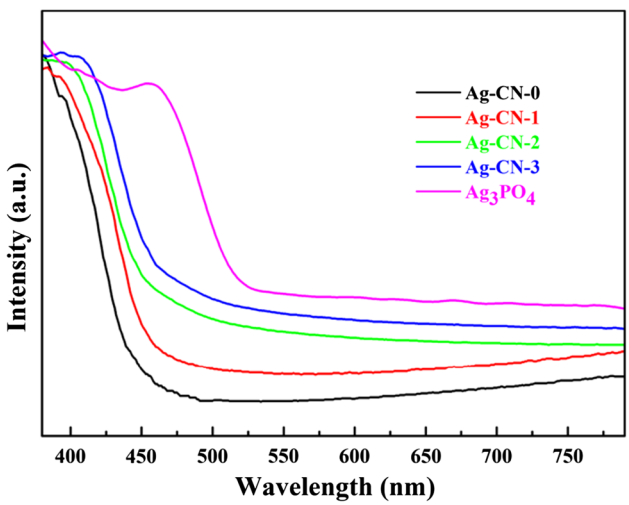

Figure 6 The UV–visible absorption spectra of Ag_3PO_4/Ag/g-C_3N_4 composites with different amount of Ag_3PO_4/Ag.

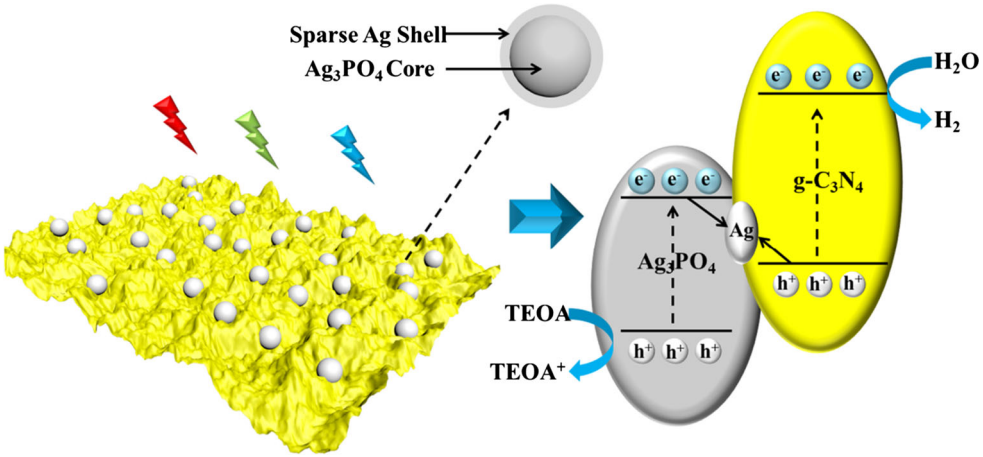

Figure 7 The schematic illustration of the hydrogen production for the Z-Scheme $Ag_3PO_4/Ag/g\text{-}C_3N_4$ nanosheets composites under visible light.

and absorption enhancement are benefitted for the visible light hydrogen production.

Based on the above results, the mechanism of the photocatalytic hydrogen production is proposed as Fig. 7. Unlike the mechanism of the conventional heterojunctions, the ternary system of $Ag_3PO_4/Ag/g\text{-}C_3N_4$ composites could form unique Z-Scheme structure. Under visible illumination, the Ag shell could immediately construct a cross-linking bridge between two semiconductors and promote the recombination of electrons from the CB of Ag_3PO_4 and holes from the VB of $g\text{-}C_3N_4$, which could increase the lifetime of the remaining holes on the VB of Ag_3PO_4 and electrons in the CB of $g\text{-}C_3N_4$ [37], that could be proved by the photoluminescence of the pure $g\text{-}C_3N_4$ and $Ag_3PO_4/Ag/g\text{-}C_3N_4$ (the PL is shown in ESI Fig. S2). Compared with other samples, the Ag-CN-X is simply mixed with Ag_3PO_4/Ag and has not formed the Z-Scheme structure, so the photocatalytic activity is similar as the pure $g\text{-}C_3N_4$, which proves the Z-Scheme again and is considered as the main reason for the enhancement of the visible light hydrogen production. It is interesting that the sample of Ag-CN-3 exhibits a decrease, which could be ascribed to that the Ag_3PO_4/Ag would result in a competition for visible light absorption in spite of itself having no hydrogen production ability [40]. Additionally, the lamellar structure of the $g\text{-}C_3N_4$ is considered as another important reason, which could provide large surface area for the growth of the Ag_3PO_4/Ag and the photocatalytic hydrogen production. What is more, the Ag^0 covers on the surface of the Ag_3PO_4 can trap the photo-generated electrons and thus inhibit the further decomposition of Ag_3PO_4, which could enhance the stability of photocatalytic hydrogen production [36, 41, 42].

Combined with the above advantages, the $Ag_3PO_4/Ag/g\text{-}C_3N_4$ composites show the excellent photocatalytic hydrogen production activity.

Conclusion

We have successfully prepared the $Ag_3PO_4/Ag/g\text{-}C_3N_4$ nanosheets composites through simple processes and proved its excellent visible light photocatalytic property in hydrogen production. The main reason could be attributed to the Z-Scheme structure of the $Ag_3PO_4/Ag/g\text{-}C_3N_4$, because the Ag shell could act as recombination center to quench the photo-generated electrons (from the CB of Ag_3PO_4) and holes (from the VB of $g\text{-}C_3N_4$), which could increase the lifetime of the remaining holes (on the VB of Ag_3PO_4) and electrons (in the CB of $g\text{-}C_3N_4$) to promote the separation of the photo-generated electron–hole pairs for increasing the photocatalytic hydrogen production property. In addition, the lamellar structure of the $g\text{-}C_3N_4$ could provide plenty of reactive sites and the sparse Ag shell on the surfaces could prevent the degradation of the Ag_3PO_4 for improving the stability of the photocatalysis are also significant reasons.

These $Ag_3PO_4/Ag/g\text{-}C_3N_4$ nanosheets composites with excellent visible light hydrogen production property are expected as the candidates in energy and environmental applications.

Acknowledgements

This work was supported by National Natural Science Foundation of China (Nos. 51672249, 51603187

and 91122022), Zhejiang Provincial Natural Science Foundation of China (Nos. LQ17F040004 and LY15E030011).

Electronic supplementary material: The online version of this article (doi:10.1007/s10853-017-1612-6) contains supplementary material, which is available to authorized users.

References

[1] Li SS, Ye L, Zhao WC, Zhang SQ, Mukherjee S, Ade H, Hou JH (2016) Energy-level modulation of small-molecule electron acceptors to achieve over 12% efficiency in polymer solar cells. Adv Mater 28:9423–9429

[2] Saxena A, Varun, El-Sebaii AA (2015) A thermodynamic review of solar air heaters. Renew Sustain Energy Rev 43:863–890

[3] Armaroli N, Balzani V (2007) The future of energy supply: challenges and opportunities. Angew Chem Int Edit 46:52–66

[4] Zhu K, Neale NR, Miedaner A, Frank AJ (2007) Enhanced charge-collection efficiencies and light scattering in dye-sensitized solar cells using oriented TiO_2 nanotubes arrays. Nano Lett 7:69–74

[5] Yao HF, Chen Y, Qin YP, Yu RN, Cui Y, Yang B, Li SS, Zhang K, Hou JH (2016) Design and synthesis of a low bandgap small molecule acceptor for efficient polymer solar cells. Adv Mater 28:8283–8287

[6] You ZY, Su YX, Yu Y, Wang H, Qin T, Zhang F, Shen QH, Yang H (2017) Preparation of g-C_3N_4 nanorod/$InVO_4$ hollow sphere composite with enhanced visible-light photocatalytic activities. Appl Catal B Environ 213:127–135

[7] Zhang FX, Yamakata A, Maeda K, Moriya Y, Takata T, Kubota J, Teshima K, Oishi S, Domen K (2012) Cobalt-modified porous single-crystalline $LaTiO_2N$ for highly efficient water oxidation under visible light. J Am Chem Soc 134:8348–8351

[8] Shen LJ, Luo MB, Liu YH, Liang RW, Jing FF, Wu L (2015) Noble-metal-free MoS_2 co-catalyst decorated UiO-66/CdS hybrids for efficient photocatalytic H_2 production. Appl Catal B Environ 166:445–453

[9] Zeng YP, Wang Y, Chen JW, Jiang YW, Kiani M, Li BQ, Wang RL (2016) Fabrication of high-activity hybrid $NiTiO_3$/g-C_3N_4 heterostructured photocatalysts for water splitting to enhanced hydrogen production. Ceram Int 42:12297–12305

[10] Xu J, Zhang LW, Shi R, Zhu YF (2013) Chemical exfoliation of graphitic carbon nitride for efficient heterogeneous photocatalysis. J Mater Chem A 1:14766–14772

[11] Zheng Y, Jiao Y, Zhu YH, Li LH, Han Y, Chen Y, Du AJ, Jaroniec M, Qiao SZ (2014) Hydrogen evolution by a metal-free electrocatalyst. Nat Commun 5:3783

[12] Ge L, Han CC, Liu J (2011) Novel visible light-induced g-C_3N_4/Bi_2WO_6 composite photocatalysts for efficient degradation of methyl orange. Appl Catal B Environ 108:100–107

[13] Zhang JY, Wang YH, Jin J, Zhang J, Lin Z, Huang F, Yu JG (2013) Efficient visible-light photocatalytic hydrogen evolution and enhanced photostability of core/shell CdS/g-C_3N_4 nanowires. ACS Appl Mater Interfaces 5:10317–10324

[14] Li YF, Jin RX, Fang X, Yang Y, Yang M, Liu XC, Xing Y, Song SY (2016) In situ loading of Ag_2WO_4 on ultrathin g-C_3N_4 nanosheets with highly enhanced photocatalytic performance. J Hazard Mater 313:219–228

[15] Li WB, Feng C, Dai SY, Yue JG, Hua FX, Hou H (2015) Fabrication of sulfur-doped g-C_3N_4/Au/CdS Z-scheme photocatalyst to improve the photocatalytic performance under visible light. Appl Catal B 168:465–471

[16] Xue JJ, Ma SS, Zhou YM, Zhang ZW, He M (2015) Facile photochemical synthesis of Au/Pt/g-C_3N_4 with plasmon-enhanced photocatalytic activity for antibiotic degradation. ACS Appl Mater Interfaces 7:9630–9637

[17] Hao RR, Wang GH, Tang H, Sun LL, Xu C, Han DY (2016) Template-free preparation of macro/mesoporous g-C_3N_4/TiO_2 heterojunction photocatalysts with enhanced visible light photocatalytic activity. Appl Catal B Environ 187:47–58

[18] Karimi-Nazarabad M, Goharshadi EK (2017) Highly efficient photocatalytic and photoelectrocatalytic activity of solar light driven WO_3/g-C_3N_4 nanocomposite. Solar Energy Mater Solar Cells 160:484–493

[19] Xu XX, Liu G, Randorn C, Irvine JTS (2011) g-C_3N_4 coated $SrTiO_3$ as an efficient photocatalyst for H_2 production in aqueous solution under visible light irradiation. Int J Hydrog Energy 36:13501–13507

[20] Ge L, Han CC, Liu J (2011) Novel visible light-induced g-C_3N_4/Bi_2WO_6 composite photocatalysts for efficient degradation of methyl orange. Appl Catal B Environ 108:100–107

[21] Cao SW, Liu XF, Yuan YP, Zhang ZY, Liao YS, Fang J, Loo SCJ, Sum TC, Xue C (2014) Solar-to-fuels conversion over In2O3/g-C3N4 hybrid photocatalysts. Appl Catal B Environ 147:940–946

[22] Ma JF, Liu Q, Zhu LF, Zou J, Wang K, Yang MR, Komarneni S (2016) Visible light photocatalytic activity enhancement of Ag_3PO_4 dispersed on exfoliated bentonite for

degradation of rhodamine B. Appl Catal B Environ 182:26–32

[23] Zhu CS, Zhang L, Jiang B, Zheng JT, Hu P, Li SJ, Wu MB, Wu WT (2016) Fabrication of Z-scheme Ag_3PO_4/MoS_2 composites with enhanced photocatalytic activity and stability for organic pollutant degradation. Appl Surf Sci 377:99–108

[24] Yang XF, Qin JL, Jiang Y, Chen KM, Yan XH, Zhang D, Li R, Tang H (2015) Fabrication of P25/Ag_3PO_4/graphene oxide heterostructures for enhanced solar photocatalytic degradation of organic pollutants and bacteria. Appl Catal B Environ 166:231–240

[25] Liu L, Qi YH, Lu JR, Lin SL, An WJ, Liang YH, Cui WQ (2016) A stable Ag_3PO_4@ g-C_3N_4 hybrid core@ shell composite with enhanced visible light photocatalytic degradation. Appl Catal B Environ 183:133–141

[26] He YM, Zhang LH, Teng BT, Fan MH (2014) New application of Z-scheme Ag_3PO_4/g-C_3N_4 composite in converting CO_2 to fuel. Environ Sci Tech 49:649–656

[27] Xiang QJ, Lang D, Shen TT, Liu F (2015) Graphene-modified nanosized Ag_3PO_4 photocatalysts for enhanced visible-light photocatalytic activity and stability. Appl Catal B Environ 162:196–203

[28] Lu JS, Wang YJ, Liu F, Zhang L, Chai SN (2017) Fabrication of a direct Z-scheme type WO_3/Ag_3PO_4 composite photocatalyst with enhanced visible-light photocatalytic performances. Appl Surf Sci 393:180–190

[29] Wan J, Du X, Liu EZ, Hu Y, Fan J, Hu XY (2017) Z-scheme visible-light-driven Ag_3PO_4 nanoparticle@MoS_2 quantum dot/few-layered MoS_2 nanosheet heterostructures with high efficiency and stability for photocatalytic selective oxidation. J Catal 345:281–294

[30] Wang ZL, Lv JL, Dai K, Lu LH, Liang CH, Geng L (2016) Large scale and facile synthesis of novel Z-scheme Bi_2MoO_6/Ag_3PO_4 composite for enhanced visible light photocatalyst. Mater Lett 169:250–253

[31] Yang ZM, Huang GF, Huang WQ, Wei JM, Yan XG, Liu YY, Jiao C, Wan Z, Pan AL (2014) Novel Ag_3PO_4/CeO_2 composite with high efficiency and stability for photocatalytic applications. J Mater Chem A 2:1750–1756

[32] Tang CN, Liu EZ, Wan J, Hu XY, Fan J (2016) Co_3O_4 nanoparticles decorated Ag_3PO_4 tetrapods as an efficient visible-light-driven heterojunction photocatalyst. Appl Catal B Environ 181:707–715

[33] Liu K, Bai YC, Zhang L, Yang ZB, Fan QK, Zheng HQ, Yin YD, Gao CB (2016) Porous Au-Ag nanospheres with high-density and highly accessible hotspots for SERS analysis. Nano Lett 16:3675–3681

[34] Song QW, Peng MS, Wang L, He DC, Ouyange J (2016) A fluorescent aptasensor for amplified label-free detection of adenosine triphosphate based on core–shell Ag@ SiO_2 nanoparticles. Biosens Bioelectron 77:237–241

[35] Tateishi I, Katsumata H, Suzuki T, Kaneco S (2017) Z-scheme photocatalytic activity of g-C3N4/tetrahedral Ag3PO4 hybrids under visible light. Mater Lett 201:66–69

[36] Pan JQ, Cao J, Mei J, Zhang XF, Wang S, Zheng YY, Cui C, Li CR (2016) The preparation of Ag@AgCl modified $K_2Ta_2O_6$ and its natural light photocatalysis. Mater Lett 184:52–56

[37] Yang XF, Chen ZP, Xu JS, Tang H, Chen KM, Jiang Y (2015) Tuning the morphology of g-C_3N_4 for improvement of Z-Scheme photocatalytic water oxidation. ACS Appl Mater Interfaces 7:15285–15293

[38] Liu J, Liu Y, Liu NY, Han YZ, Zhang X, Huang H, Lifshitz Y, Lee ST, Zhong J, Kang ZH (2015) Metal-free efficient photocatalyst for stable visible water splitting via a two-electron pathway. Science 347:970–974

[39] Wang FR, Wang JD, Sun HP, Liu JK, Yang XH (2017) Plasmon-enhanced instantaneous photocatalytic activity of Au@Ag_3PO_4 heterostructure targeted at emergency treatment of environmental pollution. J Mater Sci 52:2495–2510. doi:10.1007/s10853-016-0544-x

[40] Krungchanuchat S, Ekthammathat N, Phuruangrat A, Thongtem S, Thongtem T (2017) High UV–visible photocatalytic activity of Ag_3PO_4 dodecahedral particles synthesized by a simple hydrothermal method. Mater Lett 201:58–61

[41] Lan W, Chen YX, Yang ZW, Han WH, Zhou JY, Zhang Y, Wang JY, Tang GM, Wei YP, Dou W, Su Q, Xie EQ (2017) Ultraflexible transparent film heater made of ag nanowire/PVA composite for rapid-response thermotherapy pads. ACS Appl Mater Interfaces 217:591–602

[42] Li XX, Wan T, Qiu JY, Wei H, Qin FH, Wang YH, Liao YJ, Huang ZY, Tan XC (2017) In-situ photocalorimetry-fluorescence spectroscopy studies of RhB photocatalysis over Z-scheme g-C_3N_4@Ag@Ag_3PO_4 nanocomposites: A pseudo-zero-order rather than a first-order process. Appl Catal B Environ 9:6644–6651